Report on a problem studied at the UK Mathematics-in-Medicine Study Group Reading 2011
< http://www.maths-in-medicine.org/uk/2011/virus-budding/ >

Unravelling the Arenavirus Budding Mechanism

Ben Neuman[1] with
Oliver Jensen[2], Aniayam Okrinya[3], Joel Phillips[4], Colin Please[5],
David Schley[6] & Robert Whittaker[7]

[1]University of Reading (Problem Presenter)
[2]University of Nottingham
[3]Loughborough University
[4]University College London
[5]University of Southampton
[6]Institute for Animal Health
[7]University of East Anglia

Mathematics in Medicine Study Group,
University of Reading, September 2011

Abstract

An infection can begin with a single virus meeting an appropriate host cell, but disease does not usually manifest until days later when the infection has spread throughout a tissue. The rapid spread of infection is possible because each infected cell can release hundreds of new virus particles, or virions. Viruses are typically released by one of two processes: lysis, in which virions emerge as the infected cell bursts open, and budding, in which virions emerge gradually from a still living cell wrapped in a small part of the cell membrane.

The production of new virions is a critical stage in viral infection. A better understanding of how vesicle budding occurs could help in developing treatments to potential interrupt this process. The study group has identified a plausible mechanism for arenavirus proteins to induce additional curvature on the cell membrane, with an innate radius of curvature consistent with the observed size of virions. A non-dimensional mechanical model showed that it is possible to generate vesicle budding on a flat surface through local variation in curvature alone.

1 Introduction

Ebola haemorrhagic fever, HIV, H1N1 influenza, SARS and Lassa fever are caused by pleomorphic enveloped viruses, meaning that each is transmitted as a variably-sized package, wrapped in a lipid membrane taken from the host cell. Pleomorphic enveloped viruses have similar virion architectures, consisting of at least one type of membrane-embedded glycoprotein that projects out from the virion, a nucleoprotein that binds and protects the genome inside the particle, and a membrane-associated protein that links up the other components and drives the assembly and release of new virions, a poorly understood process known as budding.

Budding proteins have some common characteristics [1]. All are relatively small (< 300 amino acids), non-enzymatic, and the roughly 10^3 copies per virion are grouped as oligomers and arranged in a two-dimensional lattice. Despite a lack of structural similarity, each forms spheres of approximate diameter 100 nm (HIV, SARS and Lassa fever viruses) or filaments with hemispherical caps of approximate diameter 100 nm (Ebola and H1N1 viruses). Budding proteins are membrane-associated, although not usually trans-membrane, and the bulkiest part of each is appended to the inner leaflet of the virus membrane. Lastly, budding proteins can drive the budding process in the absence of other viral proteins, but bud more efficiently when all viral components are present.

Arenaviruses, which cause seven named types of haemorrhagic fever and are distributed worldwide have a simple pleomorphic enveloped architecture consisting of a surface glycoprotein (GP), an interior nucleoprotein (NP) and a small 90–100 amino-acid budding factor called Z [2]. Like the budding proteins of other pleomorphic enveloped viruses, Z can drive the budding process in the absence of other virus proteins, but buds most efficiently in the presence of the other viral components [3, 4]. The solution structure of Z has revealed a protein with flexible N and C-termini surrounding a RING domain structure which contains two zinc ions [5]. Newly expressed Z is soluble, but is quickly tethered to the membrane by a covalently attached myristate molecule. Despite a wealth of structural and reverse-genetics data, the mechanism by which Z causes a virion to bud remains unclear.

In a process typical of pleomorphic enveloped viruses, arenavirus proteins collect in discrete patches, approximately 200 nm in diameter, at the surface of infected cells (Figure 1). The organisation of pre-budding patches closely resembles that of budded virions in cross section (Figure 2). The patches then appear to bend the effectively planar membrane into a virus-sized sphere which then pinches off from the plasma membrane to form a

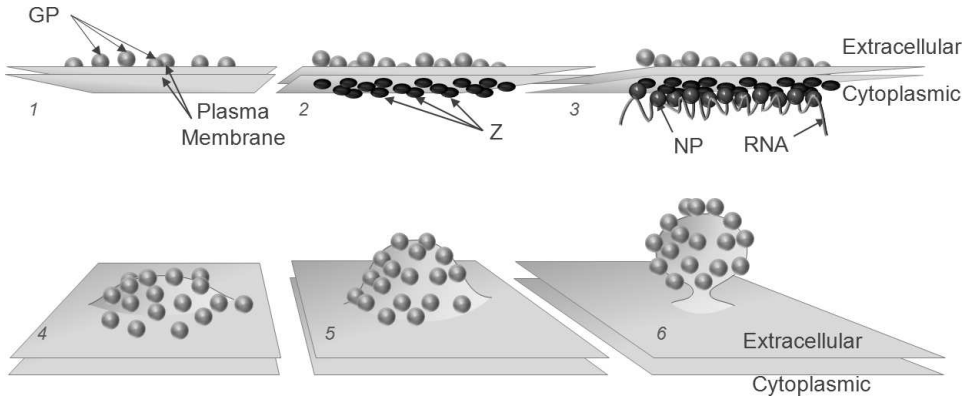

Figure 1: Schematic representation of arenavirus budding. GP naturally migrates to the cell surface (1) where it is captured by Z and arranged (2). When NP and the viral RNA genome arrive (3), the budding process (4-6) occurs.

new virion. Since Z can drive the budding process independently, this suggests that Z has membrane bending, and possibly also membrane rigidifying properties.

2 Viral budding

We propose a generalised budding mechanism in which membrane curvature is induced by a budding protein that consists of an anchor, a plug and a hook. The anchor is a secure membrane attachment point, the plug is an amphipathic region that is weakly embedded in the inner membrane leaflet, and the hook is a region that can interact with another viral or cellular component. The mechanism is simple: a tug on the hook transiently pulls the plug out of the inner leaflet of the membrane while the anchor remains firmly attached. With the plug removed, the inner leaflet takes up less space than the outer leaflet, so the membrane bends outward to compensate. If nearby plugs are pulled out at the same time, the hydrophobic faces could come together stabilise the bend. If there is no a suitable binding partner, the plug re-embeds and the membrane relaxes (Figure 3).

This model postulates regions with the functions of anchor, plug and hook, but does not specify the form each can take. For example the anchor function could be accomplished by a trans-membrane helix, a hydrophobic domain or by attachment of fatty acid molecules, as in the case of are-

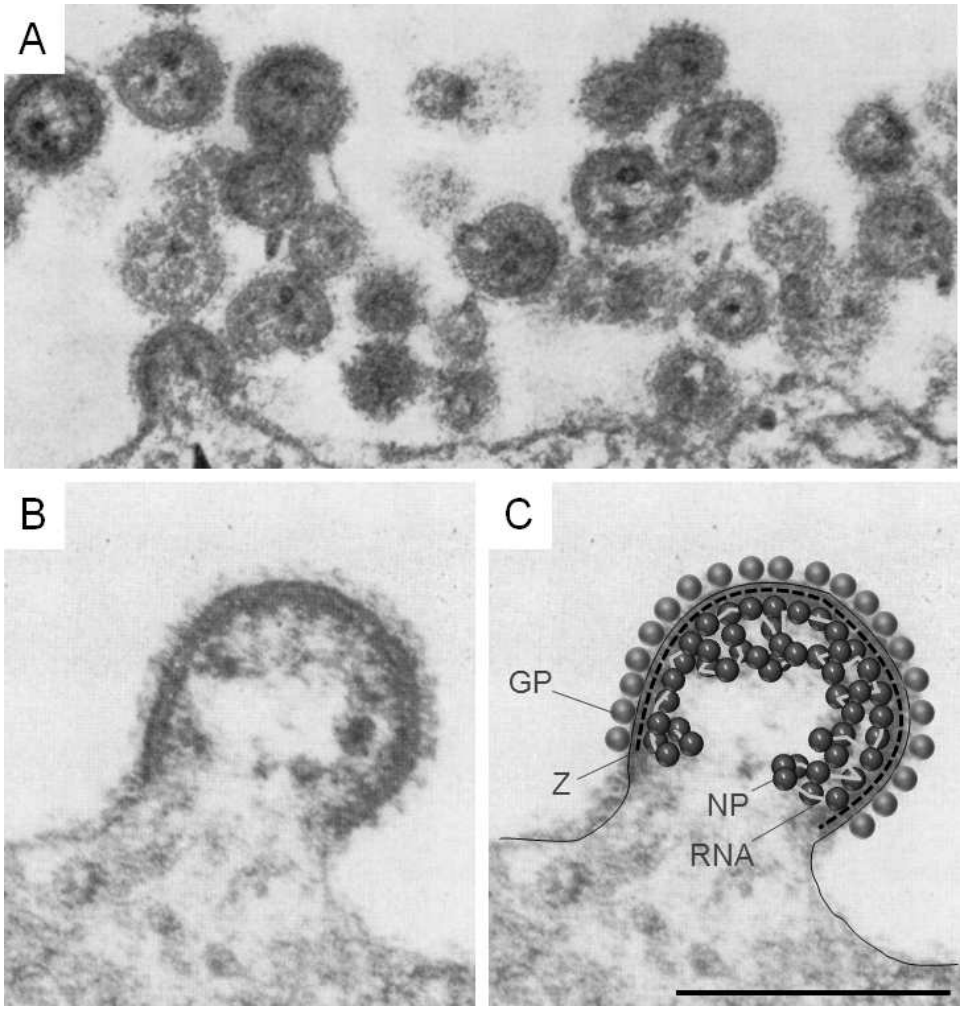

Figure 2: Electron micrographs of infected cells with budding Machupo arenavirus, adapted from [6]. Cross sectional views of emerging virions can be seen at lower left in (A) and in (B), and newly formed virions are abundant in (A). A schematic shows the arrangement of viral components in the bud (C).

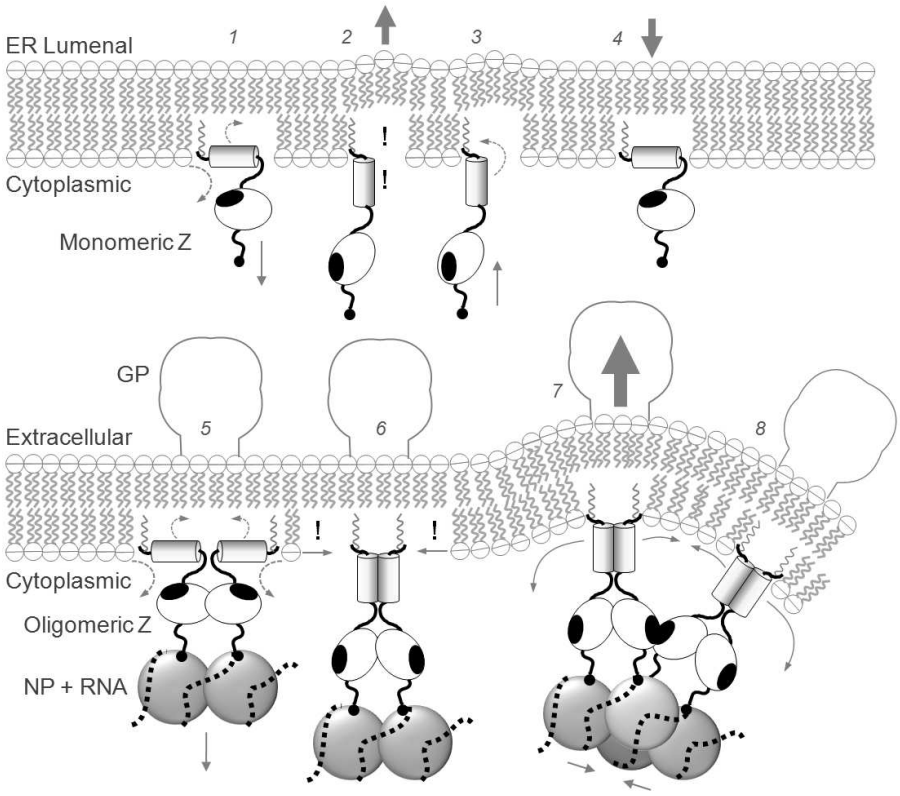

Figure 3: Anchor, plug and hook model of virus budding. Arenavirus Z is shown embedded in a lipid bilayer by means of a covalently-attached myristate (wavy line) at the N terminus, followed by an amphipathic plug (shaded cylinder) and a C-terminal hook (white oval with tail) that has a potential hook-hook interaction site (black oval). Immediately after translation (1-4), any force on the hook transiently pulls the plug out of the membrane, transiently exposing the hydrophobic face of the plug to the cytosol (!). In the context of a viral protein assembly (5-8), a simultaneous force applied to all the hooks in the assembly exposes multiple plugs, allowing the hydrophobic faces of the plugs to come together in the cytosol. This reduces the available inner leaflet area (6) leading to a bulge (7) that can be stabilised (8) by interactions between groups of proteins.

navirus Z. The plug function needs to be mechanically linked to the hook, so that force applied to the hook leads to displacement of the plug from the membrane. Thus, the plug should be near the anchor, and within pulling distance of the hook. Immediately following the myristoylation site in Z is a conserved amphipathic region that could act as a plug. Similarly, there are many possible solutions to the problem of constructing an appropriate hook, but since the virus particle needs to capture a genome in order to be infectious, the simplest solution would be to interact directly with either the RNA or the RNA-binding protein. For arenavirus, the zinc cations in the RING domain of Z form an attractive hook for negatively charged viral RNA. While we have chosen arenavirus Z as an example, budding proteins with anchor and hook functions are well attested in the literature. The amphipathic plug is the new contribution of this model, and the plausibility of the model as an explanation for the budding process hinges on the physical requirements for plug function.

3 Biological parameter estimates

In order to understand the relative length-scales of the problem, and in preparation for modelling the system, key parameter values were estimated from the literature and through expert elucidation.

The mean radius of mammalian cells r_c can be measured by direct observation using electron-microscopy (see [7, 8]). The possible thickness of the cell membrane δ is based on a lower estimate of the distance between the inner and outer phosphate groups and an upper bound of the inner and outer edge [9]. The radius of arenavirus virions r_v has been measured by electron cryomicroscopy [2].

The area of the inner membrane initially occupied by a Z-protein is based upon the dimensions of the hydrophobic segment embedded in the membrane, derived from the width of the membrane-spanning helix measured from crystal structures [10] and the incremental distance per turn in an α-helix [11].

To estimate the surface density σ of Z-proteins, we consider experimental data which suggests that these form groups of 2 [2] or 4 [12], and assume hexagonal packing across the surface of a vesicle. Experimental observations indicate a rhomboidal lattice, which is not inconsistent with this. Using the mean NP spacing distance of 8.5×10^{-9} m [13] (representative of Z-groups organisation [2]) as the side-length of a regular hexagon gives a total area of $6\frac{\sqrt{3}}{4}\left(8.5 \times 10^{-9}\right)^2$ m^2. Finally we note that hexagonal packing implies the

Parameter	Description	Value
r_c	cell radius	$(7.5\text{–}10)\ \times 10^{-6}\,\mathrm{m}$
r_v	virion radius	$(1.7\text{–}13.1)\ \times 10^{-8}\,\mathrm{m}$
δ	cell membrane thickness	$(3.4\text{–}5.0)\ \times 10^{-9}\,\mathrm{m}$
a	area removed by one Z protein	$(1.44\text{–}1.80)\ \times 10^{-18}\,\mathrm{m}^2$
σ	surface density of Z protein	n/A_g
n	number of proteins in group	2 or 4
A_g	surface area per group	$6.3 \times 10^{-17}\,\mathrm{m}^2$
B	membrane bending stiffness	$(4.4\text{–}9.0)\ \times 10^{-20}\,\mathrm{Nm}$
T_∞	cell membrane tension	$\frac{1}{2} r_c\, p_{\mathrm{tm}}$
p_{tm}	cell pressure differential	$19.6\,\mathrm{Nm}^{-2}$

Table 1: Relevant biological parameters (see text for detail).

area of the hexagon is shared by three protein groups (alternatively, the area each rhombus constructed of two triangles is equivalent to that occupied by a single protein group).

The mechanical properties of cells need to be estimated, often indirectly. Cell membrane tension can be estimated by

$$T_\infty = \frac{r_c}{2}\, p_{tm}, \tag{1}$$

where p_{tm} is the pressure differential across the membrane. Data used here is for red blood cells [14]. Estimates for the cell membrane bending stiffness are from the literature, assuming:

$$B = \frac{Eh^3}{12}, \tag{2}$$

where E is Young's modulus for the membrane [15] – see also reviews in [16] and [17].

The estimated values (used in sections 4 and 5 below) are given in Table 1.

4 Induced curvature

Of interest is the curvature that the protein binding process described in section 1 could induce on the cell membrane.

To form a vesicle of radius ρ would require a membrane region of area $4\pi\rho^2$. We consider such a region with an inner surface density of Z-proteins

σ that have been triggered. If each Z-protein removes an area a from the inner membrane, then the total amount removed underneath the region under consideration is $4\pi\rho^2\sigma a$, assuming all proteins are removed. If we form a sphere of the remaining inner membrane then this has radius $\rho - \delta$, where δ is the thickness of the membrane i.e. the distance between the inner and outer layers. Equating these gives:[1]

$$4\pi\left(\rho-\delta\right)^2 = 4\pi\rho^2 - 4\pi\rho^2\sigma a, \tag{3}$$

and solving for ρ yields:

$$\rho = \frac{\delta}{\sigma a}\Big(1 \pm \sqrt{1-\sigma a}\Big). \tag{4}$$

Only the larger of these is relevant, since $\sigma a \ll 1$ (see Table 1), and using the definition of σ and parameter estimates from Table 1 we have:

$$\rho \approx \frac{2\delta A_g}{na} = (5.95\text{–}21.9) \times 10^{-8}\,\mathrm{m}. \tag{5}$$

This matches well with the observed dimensions of arenavirus virions $r_v = 1.7\text{–}13.1 \times 10^{-8}\,\mathrm{m}$ — see Table 1 — suggesting that the curvature induced by Z-protein interaction with the inner membrane could be sufficient to explain the observed curvature of virus vesicles. In practice the inner membrane is already a little smaller than the outer membrane, due to the existing curvature of the cell, so that the predicted size would be closer still. In the next section we consider whether this mechanism alone is sufficient to generate budding on the cell surface.

5 Membrane mechanics model

5.1 Modelling assumptions

Motivated by [18], we model the cell membrane as an area-conserving inextensible shell with linear bending stiffness B. For simplicity and because we are only considering quasi-static shapes at present, we assume zero shear resistance. That is to say that the lipids that make up the membrane can slide past one another with negligible resistance.

[1] We neglect the initial difference in area of the inner and outer membranes caused by the initial curvature of the cell wall, since this $O(1/r_c)$ curvature is much smaller than the $O(1/\rho)$ curvature of the virion.

We assume that the cell is naturally spherical with radius r_c, and hence the sum of the principle curvatures of the membrane (hereinafter referred to as the 'total curvature') is $2/r_c$. We then assume that the bud formation is driven by the protein–RNA complex changing the natural total curvature to some larger value $2/\rho$, i.e. in the absence of other forces, the complex-covered area would naturally form a spherical cap of radius ρ.

To keep things simple, we assume that the protein–RNA complex forms in an axisymmetric region of area A_p and that the bud that forms will also be axisymmetric. Hence the boundary of the complex-covered region will be a circle. For bud formation we expect to need $A_p \approx 4\pi\rho^2$, and we shall assume $\rho \ll r_c$ so that the bud is small compared with the size of the cell.

Finally, as an initial step, we shall neglect any dynamic interactions with the internal and external cellular fluids, and just consider the quasi-steady evolution of the bud as the area A_p covered by the protein–RNA complex increases.

5.2 Setup and Equations

We consider an axisymmetric geometry. It most convenient to describe the membrane shape using an arc-length coordinate s measured from the centre of the bud, and an angle $\phi(s)$ that the surface makes with the horizontal.

The internal forces in the membrane are a tension $T(s)$, a bending moment $M(s)$, and a shear moment $Q(s)$. (The tension is isotropic because of the zero shear stress assumption. The bending moment is assumed to be isotropic too, as proposed by [18]. There is only one non-zero component of the shear moment by axisymmetry.) A uniform pressure difference p is assumed to act across the membrane. The various coordinates and forces are shown in figure 4.

Using simple geometry, the radial and vertical distances $r(s)$ and $z(s)$, and also to the area $A(s)$ enclosed by the circle at s can be related to s and ϕ. We find that

$$\frac{\mathrm{d}r}{\mathrm{d}s} = \cos(\phi) \ , \tag{6}$$

$$\frac{\mathrm{d}z}{\mathrm{d}s} = \sin(\phi) \ , \tag{7}$$

$$\frac{\mathrm{d}A}{\mathrm{d}s} = 2\pi r \, . \tag{8}$$

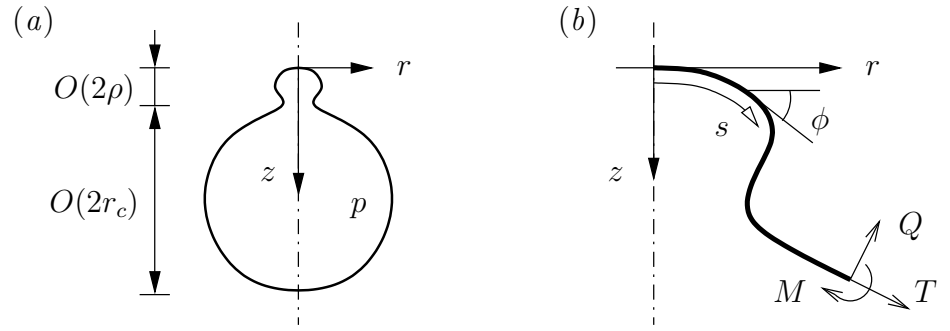

Figure 4: (a) A sketch of the axisymmetric cell with a virus bud of size $O(\rho)$ forming near $r = z = 0$ on a cell of initial radius r_c. (b) A close-up of the centre of the budding region, showing the coordinates (s, ϕ) used describe the membrane in the model. Also shown are the tension T, shear force Q, and moment M.

From [18], the two principal curvatures of the membrane are given by

$$\kappa_\phi = \frac{\mathrm{d}\phi}{\mathrm{d}s}\,, \tag{9}$$

$$\kappa_\theta = \frac{\sin\phi}{r}\,. \tag{10}$$

We denote the natural total curvature of the membrane by $\bar{\kappa}$. This takes one constant value in the area A_p covered by the complex and a lower constant value over the rest of the cell. We therefore define:

$$\bar{\kappa}(s) = \begin{cases} \dfrac{2}{\rho} & : \quad A(s) < A_p\,, \\ \dfrac{2}{r_c} & : \quad A(s) > A_p\,. \end{cases} \tag{11}$$

The bending moment M generated by the curvature is then given by the product of the bending stiffness B and the deviation from the natural total curvature, thus:

$$M = B(\kappa_\phi + \kappa_\theta - \bar{\kappa})\,. \tag{12}$$

The discontinuity in $\bar{\kappa}$ at $A(s) = A_p$ induces a discontinuity in κ_ϕ there too. In order to work with continuous variables it is convenient to define a modified curvature

$$\kappa^* = \kappa_\phi - \bar{\kappa}\,, \tag{13}$$

which will be continuous at $A = A_p$. In terms of κ^*, the moment equation (12) becomes

$$M = B\left(\kappa^* + \frac{\sin\phi}{r}\right), \tag{14}$$

and the curvature equation (9) is

$$\frac{\mathrm{d}\phi}{\mathrm{d}s} = \kappa^* + \bar{\kappa}\,. \tag{15}$$

The three equilibrium equations for the membrane, representing the balance of normal, tangential and moment forces are provided by [18].[2] From their equations (2.2)–(2.4) we take $N_\phi = N_\theta = T$ (in line with our zero shear resistance assumption), $M_\phi = M_\theta = M$ (in line with their preferred isotropic bending force assumption), $Q_\phi = Q$ (for simplicity), and write κ_ϕ in terms of κ^* using (13). Substituting for M and κ_θ using (14) and (10), the equations then become

$$\frac{\mathrm{d}}{\mathrm{d}s}\Big(Tr\Big) - T\cos\phi - Q(\kappa^* + \bar{\kappa})r = 0\,, \tag{16}$$

$$T(\kappa^* + \bar{\kappa}) + \frac{T\sin\phi}{r} + \frac{1}{r}\frac{\mathrm{d}}{\mathrm{d}s}\Big(Qr\Big) = p\,, \tag{17}$$

$$B\frac{\mathrm{d}}{\mathrm{d}s}\Big(\kappa^* r + \sin\phi\Big) - B\left(\kappa^* + \frac{\sin\phi}{r}\right)\cos\phi + Qr = 0\,, \tag{18}$$

representing: the equilibrium balance of forces in the directions of increasing s, the equilibrium balance of forces in the normal direction; and the balance of moments acting on a surface element; respectively.

The seven equations (6)–(8), and (15)–(18) form a seventh-order system for the seven unknowns r, z, A, ϕ, κ^*, Q and T as functions of s. As in [18],

[2] Axisymmetry means that the usual six equations are reduced to these three.

we can re-cast these equations as a set of explicit first-order equations:

$$\frac{\mathrm{d}r}{\mathrm{d}s} = \cos(\phi) \tag{19}$$

$$\frac{\mathrm{d}z}{\mathrm{d}s} = \sin(\phi) \tag{20}$$

$$\frac{\mathrm{d}A}{\mathrm{d}s} = 2\pi r \tag{21}$$

$$\frac{\mathrm{d}\phi}{\mathrm{d}s} = \kappa^* + \bar{\kappa} \tag{22}$$

$$\frac{\mathrm{d}Q}{\mathrm{d}s} = p - T(\kappa^* + \bar{\kappa}) - \frac{T\sin\phi}{r} - \frac{Q\cos\phi}{r} \tag{23}$$

$$\frac{\mathrm{d}T}{\mathrm{d}s} = (\kappa^* + \bar{\kappa})\, Q \tag{24}$$

$$\frac{\mathrm{d}\kappa^*}{\mathrm{d}s} = -\frac{Q}{B} + \frac{\cos\phi}{r}\left(\frac{\sin\phi}{r} - (\kappa^* + \bar{\kappa})\right) \tag{25}$$

5.3 Boundary conditions

The equations are to be solved between $s = 0$ at the centre of the bud and $s = s_{\max}$, the as-yet unknown arc length at the opposite side of the cell. The additional parameter $s_{\max}$ is to be determined as part of the solution. We therefore have a seventh-order system with one free parameter. and hence expect to have 8 boundary conditions.

The boundary conditions are

$$r = 0\,, \quad \phi = 0\,, \quad z = 0\,, \quad A = 0\,, \quad Q = 0\,, \quad \text{at} \quad s = 0\,; \tag{26}$$

$$r = 0\,, \quad \phi = \pi\,, \quad A = 4\pi r_c^2\,, \quad Q = 0\,, \quad \text{at} \quad s = s_{\max}\,; \tag{27}$$

These conditions mostly arrive from geometry and symmetry. The exceptions are $z = 0$ at $s = 0$ which arbitrarily fixes the origin of the vertical coordinate, and $A = 4\pi r_c^2$ at $s = s_{\max}$ which ensures that the total area of membrane is fixed, and equal to that of a spherical cell of radius r_c.

However, the equations are singular at $r = 0$. Therefore (numerically at least) we must apply the boundary conditions at nearby points rather than at $s = 0$ and $s = s_{\max}$ precisely. We must also expand the solution in the neighbourhood of $r = 0$ in order to count the number of constraints that the conditions actually impose. We therefore consider $s = \epsilon$ and $s = s_{\max} - \epsilon$ and look for a series solution in powers of ϵ. The most general solution that satisfies the boundary conditions on r, ϕ and Q, in the neighbourhood of

$s = (1 \mp 1)s_{\max}/2$, is found to be

$$r = \epsilon - \frac{1}{6}(\kappa_0^* + \bar{\kappa})^2\epsilon^3 + \dots\,, \tag{28}$$

$$z = z_0 \pm \frac{1}{2}(\kappa_0^* + \bar{\kappa})\epsilon^2 + \dots\,, \tag{29}$$

$$A = A_0 \pm \pi\epsilon^2 + \dots\,, \tag{30}$$

$$\phi = \pi(\tfrac{1}{2} \mp \tfrac{1}{2}) \pm (\kappa_0^* + \bar{\kappa})\epsilon \mp \frac{1}{8B}\Big(\tfrac{1}{2}p - T_0(\kappa_0^* + \bar{\kappa})\Big)\epsilon^3 + \dots\,, \tag{31}$$

$$Q = \pm\Big(\tfrac{1}{2}p - T_0(\kappa_0^* + \bar{\kappa})\Big)\epsilon + \dots\,, \tag{32}$$

$$T = T_0 + \tfrac{1}{2}(\kappa_0^* + \bar{\kappa})\Big(\tfrac{1}{2}p - T_0(\kappa_0^* + \bar{\kappa})\Big)\epsilon^2 + \dots\,, \tag{33}$$

$$\kappa^* = \kappa_0^* - \frac{3}{8B}\Big(\tfrac{1}{2}p - T_0(\kappa_0^* + \bar{\kappa})\Big)\epsilon^2 + \dots\,, \tag{34}$$

where z_0, A_0, T_0 and κ_0^* can be freely chosen. Since we started with a seventh-order system, and are left with four free constants, the boundary conditions on r, ϕ and Q impose three constraints on the system at each end.

Hence the full conditions (26) at $s = 0$ impose 5 constraints, since they require $z_0 = 0$, $A_0 = 0$, while leaving T_0 and κ_0^* free. Similarly, the full conditions (27) at $s = s_{\max}$ impose 4 constraints, since they require $A_0 = 4\pi r_c^2$, while leaving z_0, T_0 and κ_0^* free.

We therefore appear to have a total of 9 boundary conditions, making the system over-determined. However, the system has a conserved quantity

$$F = 2\pi r\Big(T\sin\phi + Q\cos\phi\Big) - \pi r^2 p\,, \tag{35}$$

which arises because of a vertical force balance.[3] The boundary conditions at $s = 0$ set $F = 0$. The conditions at $s = s_{\max}$ are consistent with this, and hence one of them is redundant.[4] We are thus back to the expected 8 conditions.

5.4 Non-dimensionalisation

We non-dimensionalise lengths using natural radius ρ of the budding region, and stresses using this length and the membrane bending stiffness B. Hence

[3] It is straightforward to show that $\mathrm{d}F/\mathrm{d}s = 0$ by using the product rule and then substituting for $\mathrm{d}(Tr)/\mathrm{d}s$ and $\mathrm{d}(Qr)/\mathrm{d}s$ from (16) and (17).

[4] It is actually slightly more complicated than this since the equations are singular at $r = 0$, and so one much consider the way in which the variables behave as they approach $r = 0$, but the general principle still applies.

we write

$$s = \rho\tilde{s}\,, \qquad r = \rho\tilde{r}\,, \qquad z = \rho\tilde{z}\,, \qquad A = \rho^2\tilde{A}\,, \qquad \phi = \tilde{\phi}\,, \tag{36}$$

$$T = \frac{B}{\rho^2}\tilde{T}\,, \qquad Q = \frac{B}{\rho^2}\tilde{Q}\,, \qquad \bar{\kappa} = \frac{1}{\rho}\tilde{\bar{\kappa}}\,, \qquad \kappa^* = \frac{1}{\rho}\tilde{\kappa}^* \tag{37}$$

Dropping the tildes, the system then becomes

$$\frac{\mathrm{d}r}{\mathrm{d}s} = \cos(\phi) \tag{38}$$

$$\frac{\mathrm{d}z}{\mathrm{d}s} = \sin(\phi) \tag{39}$$

$$\frac{\mathrm{d}A}{\mathrm{d}s} = 2\pi r \tag{40}$$

$$\frac{\mathrm{d}\phi}{\mathrm{d}s} = \kappa^* + \bar{\kappa} \tag{41}$$

$$\frac{\mathrm{d}\kappa^*}{\mathrm{d}s} = -Q + \frac{\cos\phi}{r}\left(\frac{\sin\phi}{r} - (\kappa^* + \bar{\kappa})\right) \tag{42}$$

$$\frac{\mathrm{d}Q}{\mathrm{d}s} = P - T(\kappa^* + \bar{\kappa}) - \frac{T\sin\phi}{r} - \frac{Q\cos\phi}{r} \tag{43}$$

$$\frac{\mathrm{d}T}{\mathrm{d}s} = (\kappa^* + \bar{\kappa})\,Q \tag{44}$$

where

$$\bar{\kappa}(s) = \begin{cases} 2 & : \quad A(s) < 4\pi\alpha\,, \\ \dfrac{2}{R} & : \quad A(s) > 4\pi\alpha\,, \end{cases} \tag{45}$$

and with boundary conditions

$$r = 0\,, \quad \phi = 0\,, \quad z = 0\,, \quad A = 0\,, \quad Q = 0\,, \quad \text{at} \quad s = 0\,; \tag{46}$$

$$r = 0\,, \quad \phi = \pi\,, \quad A = 4\pi R^2\,, \quad Q = 0\,, \quad \text{at} \quad s = S_{\max}\,. \tag{47}$$

The dimensionless parameters in the problem of biological relevance are the cell-to-bud size ratio

$$R = \frac{r_c}{\rho} \gg 1\,, \tag{48}$$

the dimensionless area of the membrane covered by the complex

$$\alpha = \frac{A_p}{4\pi\rho^2}\,, \tag{49}$$

and the dimensionless pressure difference

$$P = \frac{\rho^3 p}{B}\,. \tag{50}$$

Note that $\alpha = 1$ corresponds to an area covered by the complex equal to that of a sphere whose curvature is equal to the intrinsic curvature induced by the complex.

Finally, $S_{\max} = s_{\max}/\rho$ represents the dimensionless arc-length at the far side of the cell. The value of $S_{\max}$ is to be found as part of the solution of the problem, rather than it being an additional input parameter in the model.

5.5 Asymptotic solution for the budding region

For $R \gg 1$ we expect the region disturbed by the budding to only be a small fraction of the total surface area of the cell membrane. Away from the forming bud, the cell surface is expected to be spherical to good approximation with uniform curvature $\kappa^* = \kappa^*_\infty \approx 1/R$ and tension $T = T_\infty$. For consistency with the equations, we then require $P = 2T_\infty \kappa^*_\infty$.

We now consider a solution of the system (38)–(44) just for the budding region. So as $s \to \infty$ we want the solution to tend to the uniform sphere to match with the rest of the cell. Since $R \gg 1$, we have $\kappa^*_\infty = 0$ and $P = 0$ to leading order, and

$$\bar{\kappa}(s) = \begin{cases} 2 & : \quad A(s) < 4\pi\alpha \\ 0 & : \quad A(s) > 4\pi\alpha \end{cases} \tag{51}$$

The boundary conditions are then the original conditions (26)

$$r = 0\,, \quad \phi = 0\,, \quad z = 0\,, \quad A = 0\,, \quad Q = 0\,, \quad \text{at} \quad s = 0\,, \tag{52}$$

together with

$$\kappa^* \to 0\,, \quad \phi \to 0\,, \quad Q \to 0\,, \quad T \to T_\infty \quad \text{as} \quad s \to \infty\,. \tag{53}$$

By conducting a linear analysis about the uniform far-field state, we see that the set of conditions at infinity is equivalent to 2 constraints. Together with the 5 constraints at $s = 0$ we therefore have a total 7 of boundary conditions for a seventh-order system with no free parameters. (This time the conserved quantity F does not reduce the effective number of boundary conditions.)

5.6 Numerical solution and results

The system to be solved is a two-point boundary-value problem comprising seven coupled first-order ODEs. The seven variables r, z, A, ϕ, κ^*, Q and T are to be found as functions of s between $s = 0$ and $s = \infty$. There is a two-dimensional parameter space (α, T_∞) to explore, corresponding to different sizes of the complex region and different cell membrane tensions.

Numerically, we used a shooting technique to solve the system. Because the equations are singular at $s = 0$ we must use the expansions (28)–(34) to start the integration from $s = \epsilon$ rather than $s = 0$. The non-dimensional equivalents of (28)–(34) appropriate for $s = \epsilon$ in the asymptotic limit are

$$r = \epsilon\,, \tag{54}$$

$$z = \frac{1}{2}(\kappa_0^* + \bar{\kappa})\epsilon^2\,, \tag{55}$$

$$A = \pi\epsilon^2\,, \tag{56}$$

$$\phi = (\kappa_0^* + \bar{\kappa})\epsilon\,, \tag{57}$$

$$Q = -T_0(\kappa_0^* + \bar{\kappa})\epsilon\,, \tag{58}$$

$$T = T_0 - \tfrac{1}{2}T_0(\kappa_0^* + \bar{\kappa})^2\epsilon^2\,, \tag{59}$$

$$\kappa^* = \kappa_0^* + \frac{3}{8}T_0(\kappa_0^* + \bar{\kappa})\epsilon^2\,, \tag{60}$$

accurate to $O(\epsilon^2)$. We are left with two unknowns T_0 and κ_0 to chose in order to satisfy the conditions at infinity.

The conditions (53) at infinity are applied at a large but finite value $s = S$. Typically we choose $S = 20$ or $S = 30$. While there are four individual conditions, we may only impose two constraints numerically as there are only two unknown parameters in the $s = 0$ conditions. It can be see from (38)–(44) that imposing $\phi \to 0$ will also enforce $\kappa^* \to 0$, $Q \to 0$ and $\mathrm{d}T/\mathrm{d}s \to 0$. So we attempted to apply $\phi = 0$ and $T = T_\infty$ at $s = S$.

We used a `c++` shooting program, which employed Runge–Kutta integration and Newton's method, based on algorithms from Numerical Recipes [19]. However, this shooting code appeared to be unstable with respect to the $T = T_\infty$ condition. So instead, for each α, we chose an arbitrary value of T_0 and shot to achieve $\phi = 0$ at $s = S$ by varying κ_0^*. This then gave T_∞ as an output, and the solution obtained is valid for that particular value of T_∞.

We intended to repeat this for multiple values of T_0 in order to span a range of T_∞-space. However, we quickly noticed that the value of T_∞ obtained using this approach was almost exactly the input value T_0. It was discovered later that the system (38)–(44) with the boundary conditions

(52) and $T = T_0$ at $s = 0$ enforces the following pair of exact relationships

$$Q = -T_0 \sin\phi\,, \qquad T = T_0 \cos\phi\,. \tag{61}$$

Hence we have $T_0 = T_\infty$ exactly as $\phi = 0$ at both ends of the domain. (Details of the calculations leading to (61) are omitted here for brevity.)

We are thus able to use the shooting code to find solutions for any (α, T_∞) pair, by taking $T_0 = T_\infty$ and shooting to find the value of κ_0^* that achieves $\phi = 0$ at $s = S$. Matlab is then used to repeat the integration (using the complete set of initial conditions at $s = \epsilon$) in order to provide visualisation of the results. Some example solutions are shown in figure 5, with a 3D views of the membrane forming the bud in figure 6.

We see that a distinct bud-shaped region has formed at $\alpha = 1$, but it is not yet quite closed off. A slightly larger area of the cell membrane must be covered by the complex for pinch-off to occur. This is to be expected, since the rest of the cell membrane (though bending and tension forces) is attempting to pull the bud open and flat, thus resiting its formation.

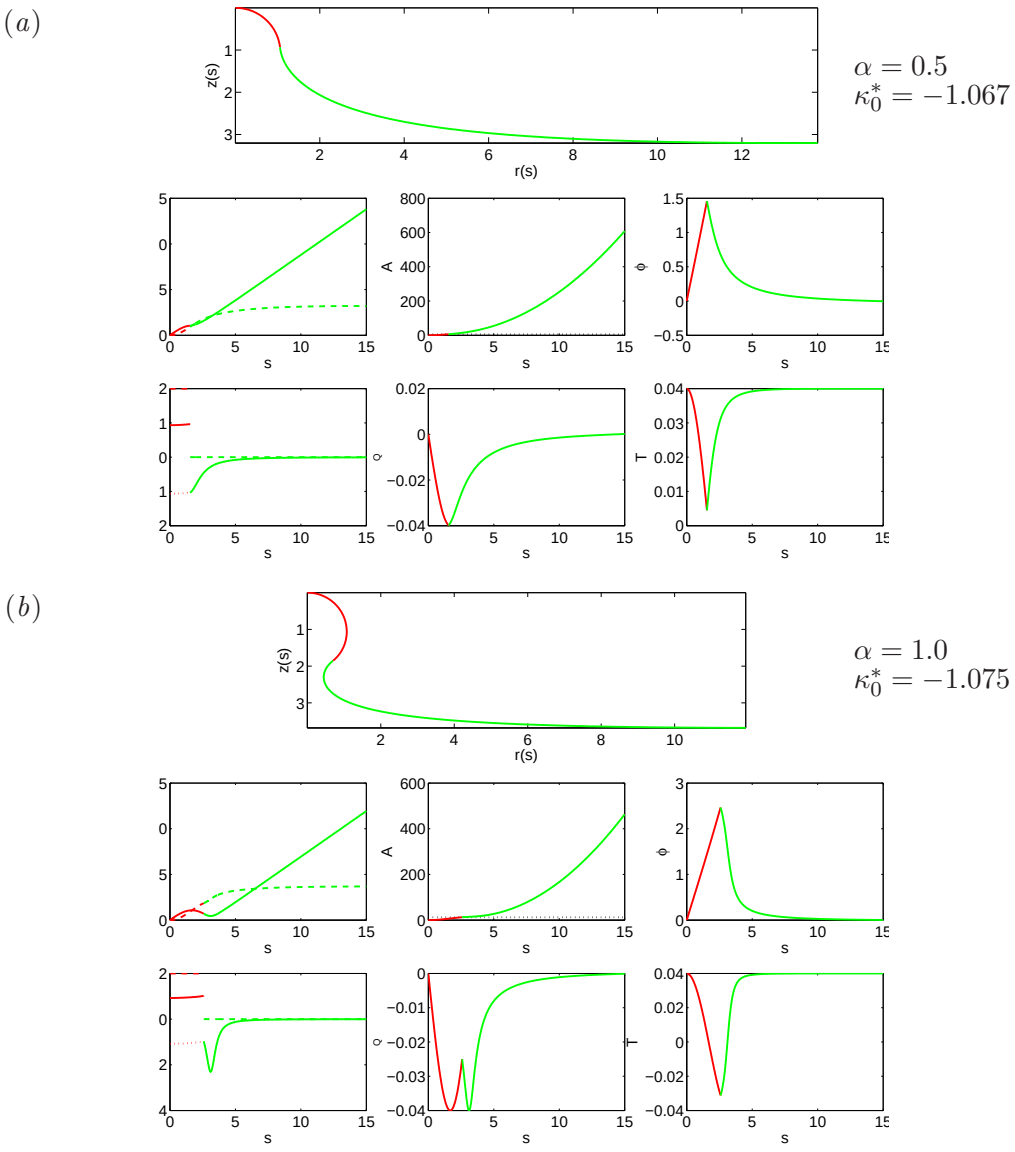

Figure 5: Numerical solutions to the asymptotic system (38)–(44) and (51)–(53) with $\epsilon = 0.01$, $S = 25$ and tension $T_0 = T_\infty = 0.04$, for different values of the covered area α. The two colours show the regions with and without additional intrinsic curvature from the complex.

(c)

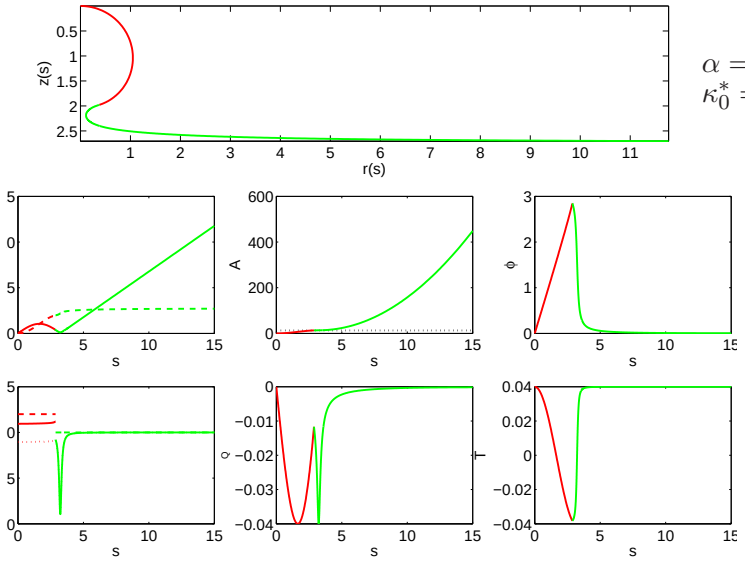

$\alpha = 1.05$
$\kappa_0^* = -1.054$

Figure 5: continued. See above for caption.

(a) $\alpha = 0.5$

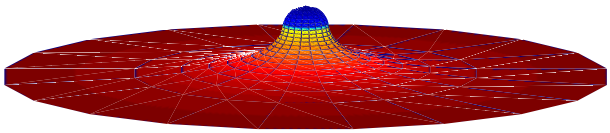

(b) $\alpha = 1.0$

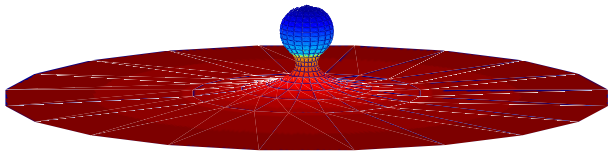

(c) $\alpha = 1.05$

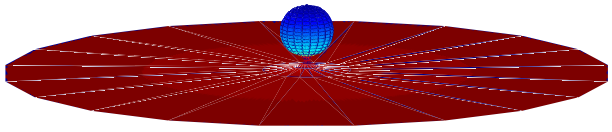

Figure 6: Numerical solutions for the three-dimensional shape of the cell membrane around the area of the budding vesicle. The parameter values are the same as those in figure 5.

6 Discussion and Conclusions

The production of new virions is a critical stage in viral infection. A better understanding of how vesicle budding occurs could help in developing treatments to potential interrupt this process.

The study group has identified a plausible mechanism for Arena virus proteins to induce additional curvature on the cell membrane. Parameter estimates from the literature indicate that the radius of curvature induced is consistent with the observed size of virions. A mechanical model is presented that shows that it is theoretically possible to generate vesicle budding on the flat surface through induced curvature alone. Limitations of our current numerical method mean that we were unable to track the solution all the way to pinch-off, but in any case, there will be additional mechanisms, such as lipid attraction between opposing sections of the bud neck, that complete the process.

Future work will focus on applying biologically relevant parameter values to the non-dimensional mechanical model. We will also validate that the system of equations has the correct number of boundary conditions. A clear extension of the model is to consider the possibility that the complex alters the bending stiffness B of the cell membrane as well as the natural curvature $\bar{\kappa}$. Predictions of what additional stiffness, if any, is required to induce budding may help estimate the energy of molecular interactions between viral proteins and the membrane.

References

[1] Neuman, B. W., Kiss, G., Kunding, A. H., Bhella, D., Baksh, M. F., Connelly, S., Droese, B., Klaus, J. P., Makino, S., Sawicki, S. G., Siddell, S. G., Stamou, D. G., Wilson, I. A., Kuhn, P. & Buchmeier, M. J. A structural analysis of M protein in coronavirus assembly and morphology. *J. Struct. Biol. 174* (2011), 11–22.

[2] Neuman, B. W., Adair, B. D., Burns, J. W., Milligan, R. A., Buchmeier, M. J. & Yeager, M. Complementarity in the supramolecular design of arenaviruses and retroviruses revealed by electron cryomicroscopy and image analysis. *J. Virol. 79* (2005), 3822–3830.

[3] Allison Groseth, S. W., Strecker, T., Hoenen, T. & Becker, S. Efficient budding of the Tacaribe virus matrix protein Z requires the nucleoprotein. *J. Virol. 84* (2010), 3603–3611.

[4] Lee, K. J., Perez, M., Pinschewer, D. D. & de la Torre, J. C. Identification of the lymphocytic choriomeningitis virus (LCMV) proteins required to rescue LCMV RNA analogs into LCMV-like particles. *J Virol 76* (2002), 6393–6397.

[5] Volpon, L., Osborne, M. J., Capul, A. A., de la Torre, J. C. & Borden, K. L. B. Structural characterization of the z ring-eif4e complex reveals a distinct mode of control for eIF4E. *Prc. Natl Acad. Sci. 107* (2010), 5441–5446.

[6] Murphy, F. A., Webb, P. A., Johnson, K. M. & Whitfield, S. G. Morphological comparison of machupo with lymphocytic choriomeningitis virus: basis for a new taxonomic group. *J. Virol. 4* (1969), 535–541.

[7] Han, Y., Liu, X.-M., Liu, H., Li, S.-C., Wu, B.-C., Ye, L.-L., Wang, Q.-W. & Chen, Z.-L. Cultivation of recombinant Chinese hamster ovary cells grown as suspended aggregates in stirred vessels. *J. Biosci. Bioengr 102*, 5 (2006), 430–435.

[8] Zhao, L., Kroenke, C., Song, J., Piwnica-Worms, D., Ackerman, J. & Neil, J. Intracellular water-specific MR of microbead-adherent cells: the HeLa cell intracellular water exchange lifetime. *NMR Biomed. 21*, 2 (2008), 159–164.

[9] Nagle, J. F. & Tristram-Nagle, S. Structure of lipid bilayers. *Biochim. Biophys. Acta 1469*, 3 (2000), 159–195.

[10] Takamori, S., Holt, M., Stenius, K., Lemke, E., Grønborg, M., Riedel, D., Urlaub, H., Schenck, S., Brügger, B., Ringler, P., Müller, S., B., R., F., G., Hub, J., De Groot, B., Mieskes, G., Moriyama, Y., Klingauf, J., Grubmüller, H., Heuser, J., Wieland, F. & Jahn, R. Molecular anatomy of a trafficking organelle. *Cell 127*, 4 (2006), 839.

[11] Neurath, H. Intramolecular folding of polypeptide chains in relation to protein structure. *J. Phys. Chem. 44*, 3 (1940), 296–305.

[12] Kentsis, A., Gordon, R. E. & Borden, K. L. B. Self-assembly properties of a model RING domain. *Prc. Natl Acad. Sci. 99*, 2 (2002), 667–672.

[13] Neuman, B. The spacing of GP, which is a better means of calculating Z area. Personal communication, 2011.

[14] Rand, R. P. & Burton, A. C. Mechanical properties of the red cell membrane: I. membrane stiffness and intracellular pressure. *Biophys. J. 4*, 2 (1964), 115–135.

[15] Niggemann, G., Kummrow, M. & Helfrich, W. The bending rigidity of phosphatidylcholine bilayers: Dependences on experimental method, sample cell sealing and temperature. *J. Phys. II France 5*, 3 (1995), 413–425.

[16] Phillips, R., Ursell, T., Wiggins, P. & Sens, P. Emerging roles for lipids in shaping membrane-protein function. *Nature 459*, 7245 (2009), 379–385.

[17] Marsh, D. Elastic curvature constants of lipid monolayers and bilayers. *Chem. Phys. Lipids 144* (2006), 146–159.

[18] Preston, S. P., Jensen, O. E. & Richardson, G. Buckling of an axisymmetric vesicle under compression: The effects of resistance to shear. *Q. J. Appl. Math. 61*, 1 (2008), 1–24.

[19] Press, W. H., Flannery, B. P., Teukolsky, S. A. & Vetterling, W. T. *Numerical Recipes: The Art of Scientific Computing.* Camb. Univ. Press, 1986.